UNIVERSITEIT•STELLENBOSCH•UNIVERSITY

jou kennisvennoot • your knowledge partner

Structural Design of a Stent for a Percutaneous Aortic Heart Valve

by

Anton Esterhuyse

Thesis presented at the University of Stellenbosch in partial fulfilment of the requirements for the degree of

Master of Mechanical Engineering

Department of Mechanical and Mechatronic Engineering
University of Stellenbosch
Private Bag X1, 7602 Matieland, South Africa

Supervisors:

Prof C. Scheffer Mr K. van der Westhuizen

March 2009

Chapter 6

Manufacturing and Electropolishing

6.1 Manufacturing of Stent Prototypes

Stent manufacturing is a highly specialised field, which involves high costs and requires advanced manufacturing equipment. As a result, for the first protoype development phase, only 10 prototype stents were manufactured for each of the two final designs selected in Section 5.10.2. The stent prototypes were laser cut courtesy of Disa Vascular (Pty) Ltd, a leading South African stent manufacturing company. Figures 6.1 and 6.2 show photos of the two designs that were selected for prototype manufacturing.

6.2 Electropolishing

6.2.1 Introduction

The manufacturing of stents by the laser cutting process results in the stents having sharp edges. It is therefore common practise in the stent manufacturing industry to electropolish stents following the cutting process. This is done to remove sharp edges and surface irregularities, to

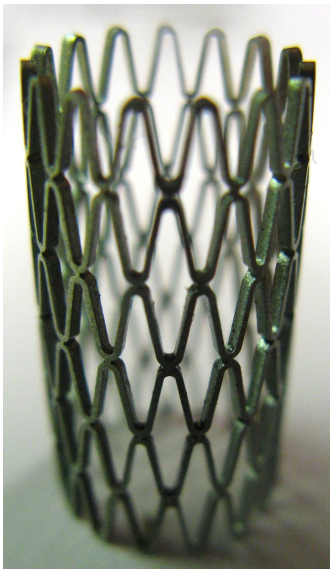

Figure 6.1: Concept A: Prototype Stent

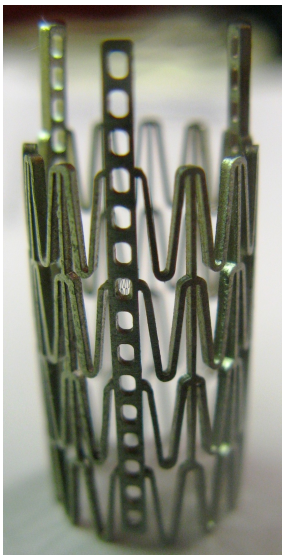

Figure 6.2: Concept B: Prototype Stent

control surface levelling and to improve surface smoothness. The process may be controlled by varying the following parameters [38]:

- Voltage potential and applied current
- Electrolite composition and concentration
- Electrolite temperature
- Processing time
- Hydrodynamics (agitation, cell configuration and geometry)
- The untreated surface quality

6.2.2 Electropolishing Parameter Setup

According to a representative of Disa Vascular (Pty) Ltd, the company's research indicated that the following electrolite composition (by weight) works well to electropolish stents manufactured from stainless steel 316L [39]:

- 40 parts: 85% Phosphoric acid
- 39 parts: 99% Glycerol
- 11 parts: Deionised water

The representative also recommended the following processing parameters as a starting point:

- Voltage potential: 15 V
- Electrolite temperature: 70 °C
- Processing time: 1-2 minutes, depending on the amount of stock removal required

Since Disa Vascular has about 10 years of experience regarding stent manufacturing and electropolishing, it was decided that their parameter recommendation would be used as a starting point for the electropolishing process.

6.2.3 Electropolishing Process Setup

Figure 6.3 shows a diagram of the setup that was used to conduct the electropolishing process.

The heated magnetic stirrer plate contains a rotating magnet which agitates the stirrer magnet placed inside the glass beaker. The electrolite temperature and agitation could therefore be controlled by the stirrer plate. A piece of thin 316L sheet metal was rolled up to form a roughly tubular structure and placed inside the beaker to act as the cathode. The stent, which acted as the anode, was suspended from a Tungsten wire into the center of the immersed cathode tube to ensure that it saw an equal electric field. The cathode tube was connected to the negative terminal and the stent to the positive terminal of a 20 V 5 A DC power supply.

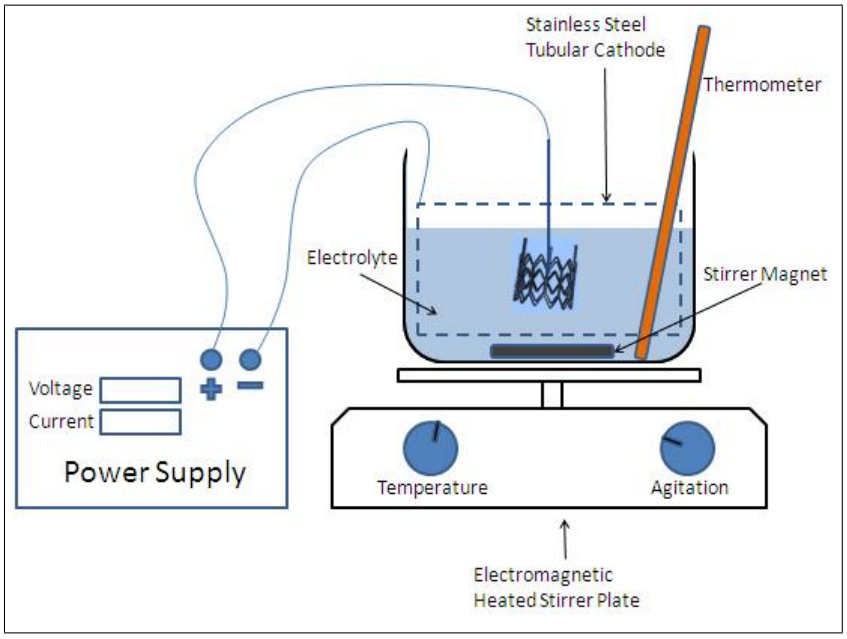

Figure 6.3: Electropolishing Process Setup

6.2.4 Electropolishing Results

Figure 6.4 shows a magnified image of a section of one of the untreated prototype stents. From the figure it can be seen that the untreated stent had a fairly poor surface finish and that the surface contained irregularities and impurities. This could be attributed to the fact that non-medical tubing was used to manufacture the stents. It was expected that, as a result of the poor untreated surface finish, the advantageous outcome of the electropolishing process would be limited.

Since the geometries of the stent designs were set, the outcome of the electropolishing process would be determined by the electrolite temperature, voltage potential, agitation and processing time. Since these four parameters could yield an endless number of possible combinations, it was decided that the agitation and voltage potential would be set, while the temperature and processing time would be varied in an attempt to achieve satisfactory electropolishing results. A number of tubing off-cut samples were used to experiment with the variable parameters. The results of these experiments are presented in Appendix D. The results of

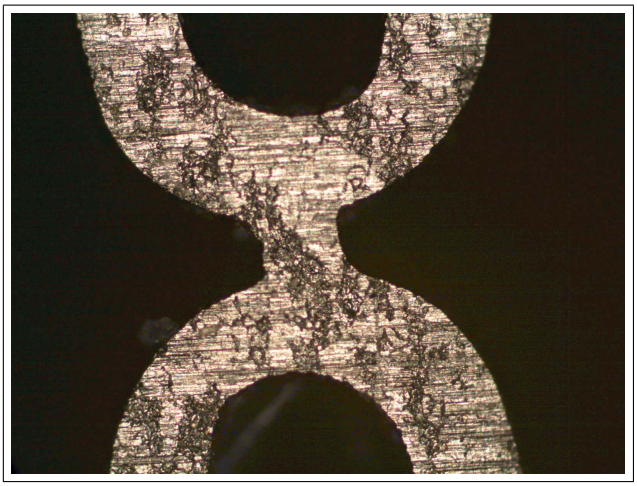

Figure 6.4: Untreated Stent - 100x Magnification

these samples indicated that pitting (formation of crevices) of the surface started immediately at the onset of the electropolishing process and was unavoidable. It appeared that this may be attributed to the poor untreated surface finish. It also appeared as though a variation in temperature had a greater influence on the results as compared to a variation in processing time. The results of the samples were used as a basis to investigate the parameters that would give the best possible surface finishes for the prototype stents. The aim was to brighten the surface and smoothen the edges without compromising the stent structure. The parameters that worked best for the stent prototypes are given in Table 6.1. Figures 6.5 and 6.6 show magnified sections of stent prototypes that were electropolished with these parameters.

Although the results obtained are far from optimal, the electropolishing process aided in smoothing the sharp stent edges, which would otherwise present a possible threat to balloon rupture as well as suture and leaflet damage. It can also be seen from the results that the processing time for Concept A is considerably higher compared to the processing time for Concept B. This could be attributed to the difference in stent geometry.

Table 6.1: Stent Prototype Electropolishing Parameters

	Voltage (V)	Agitation	Temperature (°C)	Processing Time (s)
Concept A	16	3/6	85	240
Concept B	16	3/6	78	135

Figure 6.5: Microphotograph of Concept A Prototype: Polished Surface

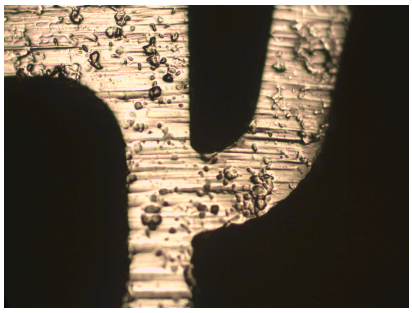

Figure 6.6: Microphotograph of Concept B Prototype: Polished Surface

6.3 Assembly of Valve Prototypes

Although the assembly of the valve prototypes did not form a part of this thesis, a photo of each of the assembled concepts is included in this section to confirm the compatibility of the concepts with the respective assembly configurations. The valve prototypes were assembled by Mr. A. Smuts as part of his Master's thesis. Figure 6.7 shows one of the prototypes that were assembled according to Concept A and Figure 6.8 shows one of the prototypes that were assembled according to Concept B.

Figure 6.7: Concept A - Assembled Prototype

Figure 6.8: Concept B - Assembled Prototype

Chapter 7

Experimental Analysis

In order to perform an initial evaluation of the performance and characteristics of the manufactured prototype stents, the discrete deformation and loading modes to which the stents will be subjected during assembly and deployment (Section 5.6) were experimentally replicated in an in-vitro environment. The experimental results also served to evaluate the reliability of the finite element simulations.

7.1 Experimental Procedure

The simulated deformation and loading modes were experimentally replicated by performing the steps described in this section. For each of the steps, the distal, proximal and central outer diameters as well as the lengths of the stents were measured at regular intervals by means of a digital vernier caliper.

7.1.1 Rigid Expansion Process

The initial rigid expansion of the stents was achieved by advancing the stents across a stainless steel polished tapered rod, which was specifically manufactured for this purpose. The diameter of the tapered rod increased from 8 mm to 20.2 mm at a taper angle of 1.06 degrees. The stents were slightly over expanded to compensate for elastic radial re-

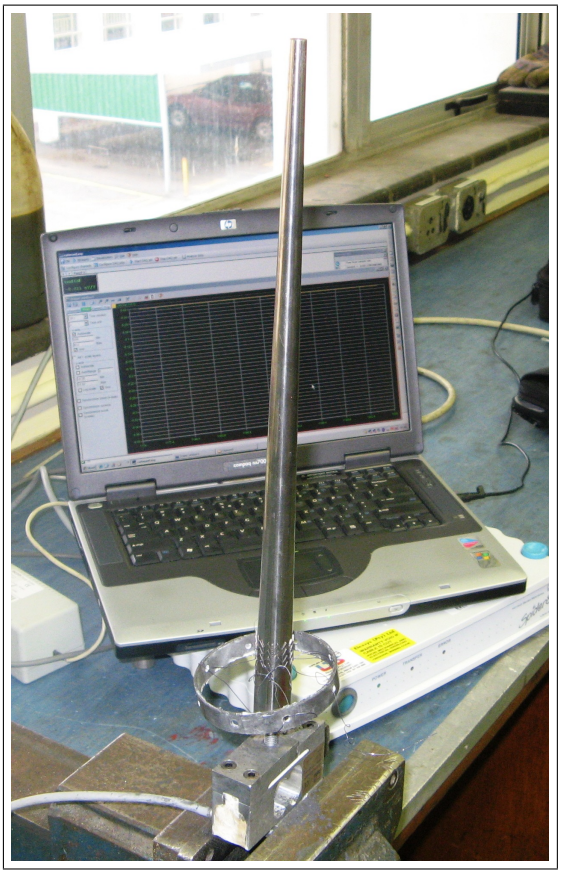

Figure 7.1: Photo of Taper Expansion Setup

coil. To achieve this process, the stents were first attached to a PVC ring with strong sutures. The PVC ring was subsequently advanced over the tapered rod to achieve an even expansion of the stents. Graphite powder was used as a lubricant. Figure 7.1 shows a photo of the setup that was used for the rigid expansion process. Figure 7.6 (Section 7.2.2) shows a diagram of the rigid expansion process.

7.1.2 Crimping Process

The crimping process was achieved by crimping the stents onto a balloon catheter by hand. The first phase of the hand crimping was achieved by crimping the stents against the tapered stainless steel rod, which served as a crimping guide. The final phase of the hand crimping was achieved

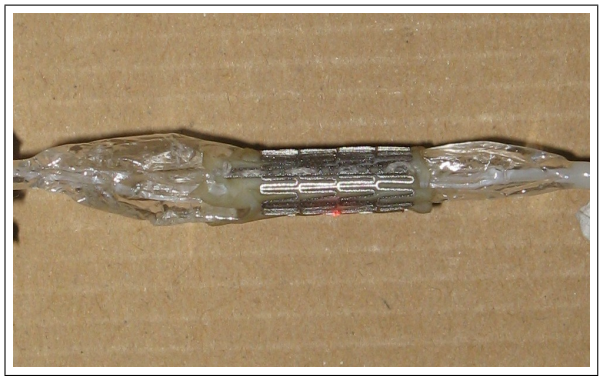

Figure 7.2: Concept B Prototype: Crimped State

by crimping the stents, over a thin pericardium sheath, onto the balloon catheter. The sheath served to represent the valve leaflets as well as protect the balloon from rupture. Figure 7.2 shows the crimped state for one of the prototypes of Concept B.

7.1.3 Deployment Process

As described in Section 7.1.2, the prototype stents were crimped onto a low-compliance NuMed^{TM} PET (polyester polyethylene terephthalate) balloon catheter with a rated deployment diameter of 18 mm and a burst pressure of 6 bar. Prior to the deployment step, the balloon catheter was filled with saline and flushed to remove any trapped air bubbles. Subsequently, the stents were gradually deployed to the deployment diameter by increasing the pressure through a syringe, which was connected to the corresponding catheter port. The deployment pressure was monitored using a pressure gage, connected to a side port. Figure 7.3 shows a photo taken during the deployment process for a prototype stent of Concept A.

7.1.4 Elastic Recoil

After the deployment process, the internal balloon pressure was removed to allow for the elastic recoil of the stents.

Figure 7.3: Concept A Prototype: Deployment Process

7.1.5 Fatigue Loading

In order to evaluate the resistance of the stents to the fatigue loads, as would be typically experienced by the stents in an in-vivo environment, it was initially proposed that the assembled valves be subjected to accelerated fatigue tests in a pulse duplicator. A pulse duplicator is a machine which simulates the pumping action of the left ventricle. The design and construction of a pulse duplicator formed part of another Master's thesis. Unfortunately, at this point in time, the pulse duplicator still experiences some technical difficulties during operation which prevents it from operating for extended periods of time. Therefore, fatigue tests could not yet be conducted and the fatigue simulations could not be validated.

7.2 Discussion of Experimental Results

7.2.1 Stent Deployment Process

Figures 7.4 and 7.5 show, for both concepts, plots of the distal outer diameters vs. deployment pressures for the experimental data as well as the simulation results. From the plots it can be seen that, for both concepts, the simulated deployment pressure is considerably higher compared to the actual required deployment pressure. It seems probable that this may be attributed to the effect of the outward vectored forces of the bulging balloon membrane, in between the struts, that is not taken into account in the finite element simulations [40]. During the actual deployment of

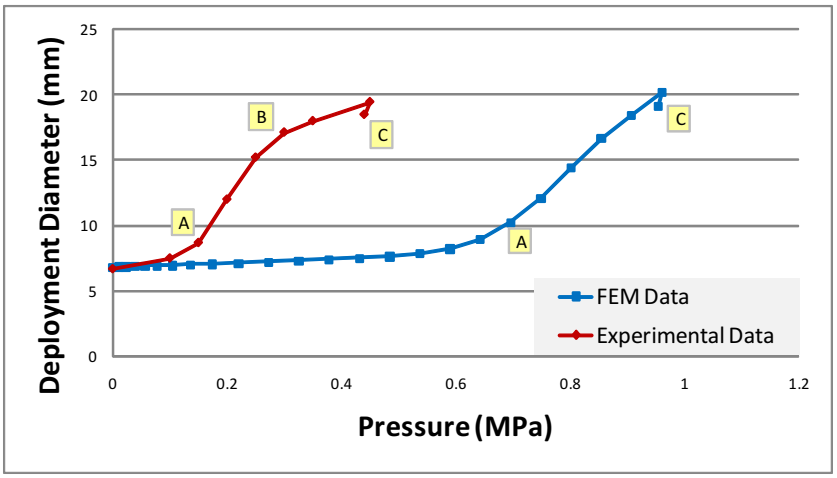

Figure 7.4: Concept A Prototype: Deployment Pressure vs. Displacement - Comparison of Results

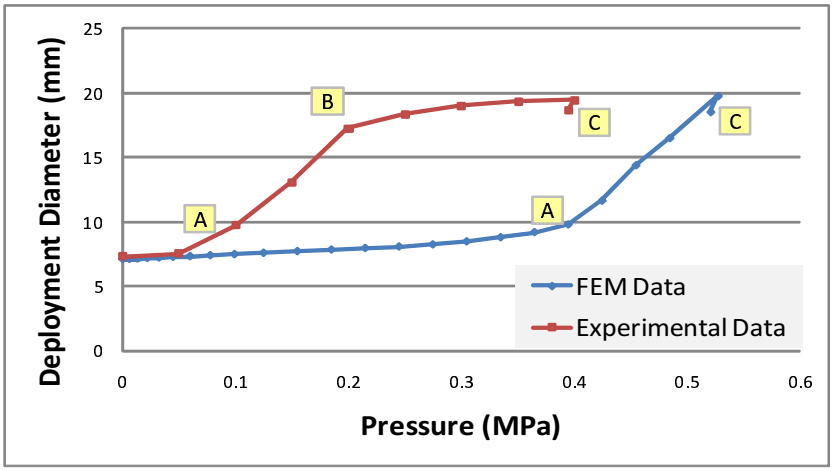

Figure 7.5: Concept B Prototype: Deployment Pressure vs. Displacement - Comparison of Results

the stent a load of unknown magnitude is transferred by the membrane to the stent as the balloon expands. The results could therefore not be used to verify the validity of the simulations.

The results could however be used to indicate the actual pressure required to deploy the stents. The experimental results confirmed that Concept A required a larger deployment pressure, as suggested by the finite element simulations. The deployment pressure for Concept A was

0.25 MPa, while the deployment pressure for concept B was 0.2 MPa. The deployment pressure was taken as the point at which the required deployment pressure was no longer dominated only by the resistance from the stents, but also by the resistance of the balloon, as it neared its nominal deployment pressure (Symbol "B" in the figures).

It should also be noted that there existed a correlation between the simulation data and experimental data for the diameters at which the stents experienced a transition from the elastic deployment deformation to plastic deployment deformation, indicated by symbol "A" in the figures.

For both the simulation and experimental data, symbol "C" indicates the amount of elastic radial recoil which takes place when the deployment pressure is removed.

7.2.2 Rigid Expansion Process

As a result of the fact that the experimental results of the deployment process failed to validate the finite element simulations, an experiment had to be designed to verify the validity of the simulations. For this purpose an experimental setup was constructed to measure the reaction force applied to the tapered expansion rod as the stents were expanded by advancing them across the rod.

For this experimental setup, the tapered rod was mounted to a 500 N load cell and the force required to advance the stents across the rod was recorded, using a SPIDER^{TM} bridge amplifier / data acquisition system, against the instantaneous translated distance along the rod. Although only a small part of the load cell range was used, a calibration test was conducted which indicated that the load cell was linear and accurate in this range. Graphite powder was used as a lubricant. Figure 7.6 shows a diagram of the experimental setup that was used.

For both stent concepts, this process was also subjected to a finite element analysis. Since the coefficient of friction between the stents and the taper was an unknown variable, the simulations for both concepts were

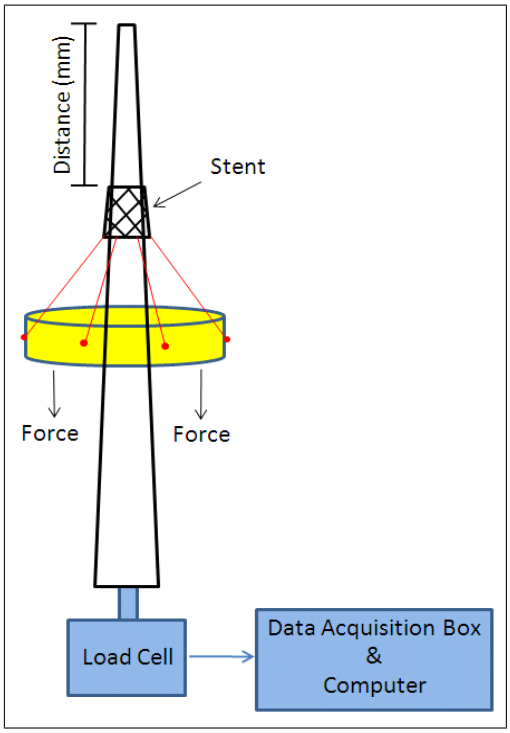

Figure 7.6: Diagram of Taper Expansion Process

conducted for different friction coefficients.

The experimental results as well as the results of the finite element simulations for different coefficients of friction are given for Concept A in Figure 7.7 and for Concept B in Figure 7.8. From these results it can be seen that for Concept A, a coefficient of friction of 0.085 correlated well with the experimental results, while for Concept B a coefficient of friction of 0.1 correlated well with the experimental results. These results indicated that the geometric models, mesh densities and material properties used to describe the FEM models could, to a certain extent, be implemented in finite element analyses to predict the behavior of the concepts.

7.2.3 Modes of Deployment

For Concept A, the "dog-boning" effect (Equation 5.7.1) is plotted as a function of central outer diameter in Figure 7.9 for both the experimental

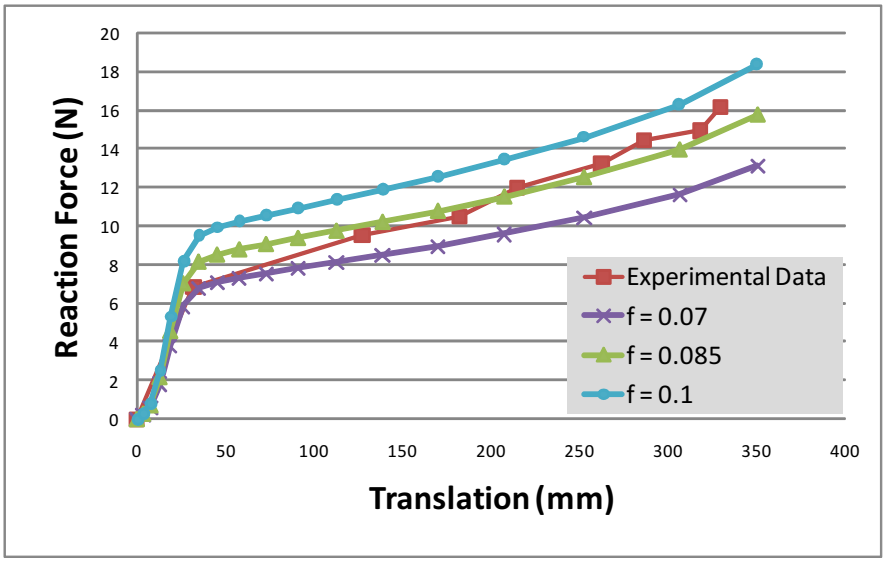

Figure 7.7: Concept A: Rigid Expansion - Comparison of Results

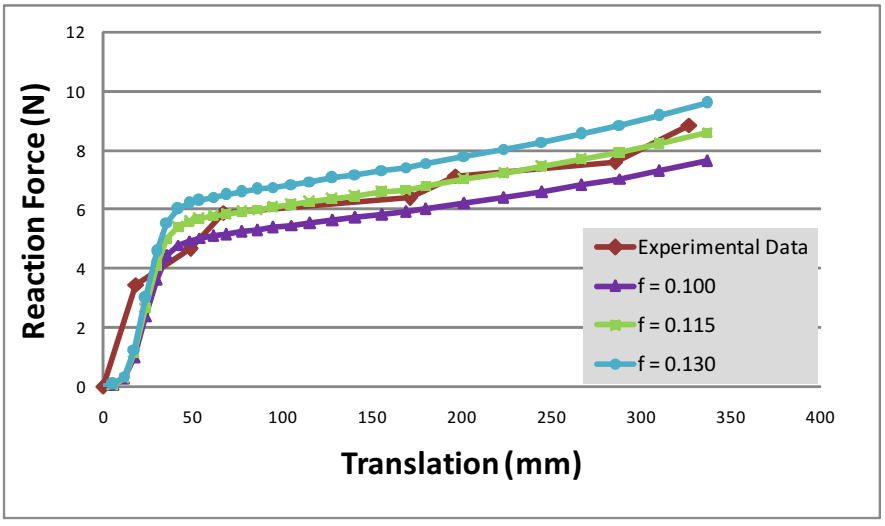

Figure 7.8: Concept B: Rigid Expansion - Comparison of Results

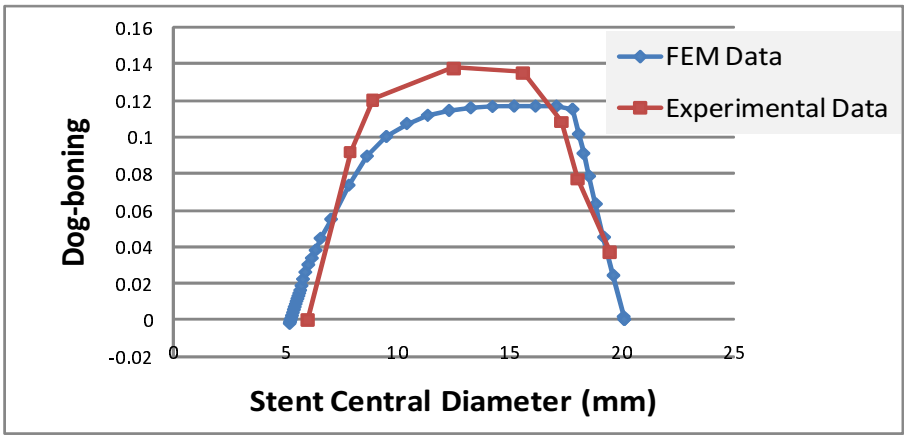

Figure 7.9: Concept A: Dog-boning - Comparison of Results

results as well as simulated results. From the figure it can be seen that the maximum dog-boning for the experimental results is somewhat higher compared to the simulation data. It is again plausible that the effect of the balloon membrane played a role in the deviation of the experimental results from the simulation data. Other factors such as non-uniform strut width may also have attributed to the discrepancy between the data sets.

For Concept B, the coning effect (Equation 5.7.2) is plotted as a function of the stent outer diameter in Figure 7.10 for both the experimental results as well as the simulated results. From the figure it can be seen that the maximum coning for the experimental results is slightly higher compared to the simulation data. Apart from the discrepancy between the maximum coning, the experimental data correlates well with the simulation data.

7.2.4 Crimp Diameter, Foreshortening and Recoil

The parameters for minimum crimp diameter, foreshortening and elastic recoil were also compared for the simulation data and experimental data. The results for the comparison is given in Table 7.1. The deviation of the simulation data from the experimental results is also given as a percentage in the table. From the comparison of the simulation data and experimental data it can be seen that the simulations predicted the min-

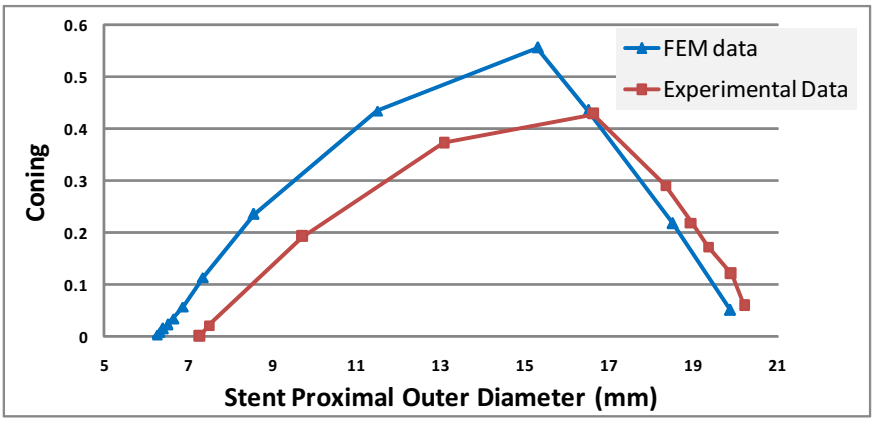

Figure 7.10: Concept B: Coning - Comparison of Results

Table 7.1: Parameter Comparison: Experimental Data vs. Simulation Data

Concept A	Simulation Results	Experimental Results	Deviation (%)
Min. Crimp Dia. (mm)	4.64	4.71	1.5
Foreshortening (%)	8.67	10.12	14.3
Radial Recoil (%)	5.53	5.20	6.3
Longitudinal Recoil (%)	-0.86	-0.92	6.5

Concept B	Simulation Results	Experimental Results	Deviation (%)
Min. Crimp Dia. (mm)	5.43	5.27	3.0
Foreshortening (%)	4.00	3.54	13.0
Radial Recoil (%)	6.30	6.03	4.5
Longitudinal Recoil (%)	-0.55	-0.49	12.2

imum crimping diameter to an accurate degree. For both concepts the parameter for foreshortening was predicted to the least accurate degree. This was unexpected as foreshortening is a geometry dependent parameter as opposed to a material dependent parameter and a higher accuracy would be expected. The parameters for recoil were predicted within an 13% margin, which, from an engineering point of view, is a reasonable deviation.

7.3 Conclusion to the Experimental Analysis

Although there were some discrepencies between the data obtained from the simulations and the experimental results, the experimental analysis served to provide a good insight into the actual performance characteristics of the concepts as well as to provide insight into the value of finite element simulations with respect to stent design and development.

From the experimental analysis, the actual required deployment pressure was determined, the mode of deployment for each concept was evaluated and other stent characteristic were measured. The knowledge gained from the experimental analysis will be invaluable for continued prototype development and refinement.

Chapter 8

Conclusion

The literature review indicated that the development of a percutaneous aortic heart valve is an intricate process which is extremely time consuming and costly. It is therefore imperative that modern technologies be implemented to reduce the number of design iterations required to develop a functional device. Since the finite element method provides an cost and time effective tool to perform structural analyses, it was the objective of this thesis to implement this technology to develop, taking into account time and cost efficiency, a first prototype for the stent component of a percutaneous aortic heart valve, which would serve as the stepping stone towards continued product development.

In order to achieve this objective a number of stent concepts were generated. The two most promising concepts were subjected to comprehensive finite element analyses of the deformations and forces experienced by the stent during implantation and operation. For each of the most promising concepts, the simulations were conducted for different strut widths to determine the strut width that would be most suited for the specific stent application. The results of the FEM simulations indicated that a variation in strut width had a substantial influence on stent characteristics such as radial strength, crimp diameter, stress and strain, elastic recoil and fatigue. Stent characteristics such as mode of deformation and foreshortening were less influenced by strut width. The results also indi-

cated that the selection of stent geometry had a major influence on stent performance.

From the results of the FEM analyses a strut width was selected for each concept and a number of prototypes were manufactured. The prototypes were subjected to experimental analyses to evaluate the relevance of the FEM analyses as well as to evaluate the actual stent performance. Although the FEM analyses were able to predict some of the stent characteristic to a fairly accurate degree, the overall performance of the stents were compromised by non-uniform strut width and poor surface finishes. The use of non-medical grade tubing resulted in non-uniform strut widths due to the fact that the laser beam had trouble maintaining a pinpoint focus on the tubing which had a low concentric tolerance. An important conclusion that may be drawn from this result is that the use of high grade medical tubing is vital for optimal stent performance.

The most significant conclusion that could be drawn from the finite element simulations and experimental work was that Concept A is the most promising stent design. For comparable strut widths, Concept A showed a lower metal-surface area ratio, a higher radial strength, a smaller crimp diameter and slightly less radial recoil. Concept A was compatibile with the parabolic leaflet assembly configuration, which is the configuration which most accurately resembles the native aortic valve. Concept A also exhibited a dog-boning deployment mode, which might be beneficial to the positioning of the device. A single drawback of Concept A was that it exhibited a greater amount of foreshortening compared to Concept B. However, testing of the prototype valves assembled by Mr. A. Smuts indicated that this was not a significant drawback.

An additional conclusion that can be drawn is that the electropolishing process failed to achieve a significant improvement of the fairly poor surface quality of the metal tubing used. As a result of this, the optimal electropolishing parameters for the specific stent geometries could not be determined.

Through the research conducted, the author gained experience in the simulation of non-linear finite element problems. A better understanding

was also achieved regarding the aspects involved in the development of a percutaneous aortic heart valve and knowledge was gained regarding the design parameters that determine stent performance characteristics.

As a step towards developing a functional product, an application for a provisional patent has been submitted for a percutaneous aortic heart valve which utilises Concept A.

Chapter 9

Limitations and Recommendations

The work done in this Master's thesis served as a stepping stone towards the development of a percutaneous aortic heart valve that will eventually be suitable for implantation in human beings. It is therefore vital that the knowledge gained through the research conducted be transferred to the entity that will continue the research and development of the device. The goal of this section is therefore to highlight the limitations of the current work as well as provide recommendations for future research on the subject.

9.1 Limitations to the Work

The following limitations to the current work were identified:

- The external environment, such as the radial reaction force exerted by the aortic annulus, was not considered for finite element simulations.
- The effect of the bulging balloon-membrane on the deployment of the stents was not considered for the finite element simulations.

- The simulations and experimental work was conducted for stainless steel instead of the more superior cobalt-chrome alloy, MP35N of L605.
- The effect of a variation in strut thickness was not considered.
- Fatigue performance of the prototypes were not evaluated in a pulse duplicator.

9.2 Recommendations

Based on the results and limitations to the work, the following recommendations can be made for continued development of a fully functional percutaneous aortic valve replacement:

- Since the results of the present work indicated that Concept A is the most promising concept, it is recommended that continued development of the prototype be focused on this concept.
- Medical grade cobalt-chrome (MP35N) tubing must be used instead of lower grade stainless steel to manufacture the prototypes.
- Since cobalt-chrome exhibits slightly superior properties compared to stainless steel, it is recommended that the design for Concept A be slightly altered prior to the next round of prototype manufacturing. It is recommended that the strut thickness and strut width be slightly reduced. Also, since the actual deployed length of the prototype stent was slightly less compared to the simulated deployed length, the overall length of the stent may be slightly increased. The suggested dimensions for the next round of prototype manufacturing is given in Figure G.1 of Appendix G. The main purpose of these alterations is to give a slight reduction in deployment stiffness, as the experimental results indicated that the present design is slightly too stiff.

- The optimal electrolyte composition and electro-polishing parameters must be determined for a prototype stent manufactured from cobalt-chrome.
- A suitable test-rig must be designed and constructed to improve the accuracy of the experimental results.
- A crimping tool must be developed that is capable of achieving the uniform crimping of the assembled prosthesis.
- A delivery system must be developed and manufactured that is compatible with the valve prosthesis being developed.
- In-vitro fatigue tests must be conducted for the assembled prototype valves.
- The animal trial phase must be initiated.

List of References

[1] Cleveland-Clinic: Catalyst news. vol 3, Issue 3. (Cited on pages xi and 3.)

[2] David Chua, S., MacDonald, B. and Hashmi, M.: Effects of varying slotted tube (stent) geometry on its expansion behavior using finite element method. *Journal of Materials Processing Technology*, vol. 155-156, pp. 1764–1771, 2004. (Cited on pages xi, 13, 14, and 15.)

[3] UK, P.: Cardiac catheterisation. 2008.
Available at: `http://www.patient.co.uk/showdoc/40000522/` (Cited on pages xi and 34.)

[4] van Aswegen et al., K.: *Dynamic Modelling of a Stented Aortic Valve*. Master's thesis, University of Stellenbosch, 2008. (Cited on pages xii, 4, 52, and 53.)

[5] Smuts, A.e.a.: *Investigation of tissue materials for implamentation in a Percutaneous Aortic Heart Valve*. Master's thesis, University of Stellenbosch, 2008. (Cited on pages xii, 4, 25, 52, and 54.)

[6] University of maryland medical center, valvular disease. 20/05/2008.
Available at: `http://www.umm.edu/heart/valve_diseases.htm` (Cited on pages 1 and 2.)

[7] Stanford hospital, valvular disease.
Available at: `http://www.stanfordhospital.com/clinicsmedservices/coe/heart/diseasesconditions/valvularheartdisease/default` (Cited on page 1.)

[8] Ye, J., Cheung, A., Lichtenstein, S., Pasupati, S., Carere, R., Thompson, C., Sinhal, A. and Webb, J.: Six-month outcome of transapical transcatheter

aortic valve replacement in the initial seven patients. *European Journal of Cardiothoracic Surgery*, vol. 31, p. 16, 2007. (Cited on page 2.)

[9] Cervantes, J.: Fiftieth anniversary of the first aortic valve prosthesis implantation. *Langenbecks Arch Surg*, vol. 388, p. 366367, 2003. (Cited on page 2.)

[10] Weich, H.: E-mail correspondecse with author, 15 october 2007. (Cited on pages 2 and 22.)

[11] Boudjemline, Y. and Bonhoeffer, P.: Steps toward percutaneous aortic valve replacement. *American Heart Association*, 2002. (Cited on pages 3 and 8.)

[12] Brodsky, A.M.: Percutaneous approaches to aortic valve replacement. *Cardiac Interventions*, December 2004. (Cited on pages 3 and 8.)

[13] Joudinaud, T.M. and Flecher, E.M.: Sutureless stented aortic valve implantation under direct vision. *J Card. Surg.*, vol. 22, pp. 13–17, 2007. (Cited on page 3.)

[14] Anderson, H., Knudsen, L. and Hasenkam, J.: Transluminal implantation of artificial heart valves. description of a new expandable aortic valve and initial results with implantation by catheter technique in closed-chest pigs. *European Heart Journal*, vol. 13, pp. 704–708, 1992. (Cited on page 8.)

[15] Lutter, G.e.a.: Percutaneous aortic valve replacement: An experimental study. i. studies on implantation. *Journal of Thoracic and Cardiovascular Surgery*, vol. 123, pp. 768–776, 2002. (Cited on page 8.)

[16] Boudjemline, Y. and Bonhoeffer, P.: Percutaneous implantation of a valve in the descending aorta in lambs. *European Heart Journal*, vol. 23, pp. 1045–1049, 2002. (Cited on page 8.)

[17] Cribier, A., Eltchaninoff, H. and Bash, A.: Percutaneous transcatheter implantation of an aortic valve prosthesis for calcific aortic stenosis. *Circulation*, vol. 106, pp. 3006–3008, 2002. (Cited on page 8.)

[18] Gilad, R. and Somogyi, R.: Percutaneous heart valves: The emergence of a disruptive technology. *University of Toronto Medical Journal*, vol. 82, pp. 200–201, 2005. (Cited on page 9.)

[19] CoreValve: Corevalve: The revalving technology. 2008.
Available at: `http://www.corevalve.com` (Cited on page 9.)

[20] Poncin, P. and Proft, J.: Stent tubing: Understanding the desired attributes. In: *Materials & Processes for Medical Devices Conference*. 2003. (Cited on pages 9, 10, 11, 21, 22, 23, and 44.)

[21] Meyer-Kobbe, C.: The importance of annealing 316 lvm stents. *Medical Device Technology*, pp. 19–21, January 2003. (Cited on page 11.)

[22] Amit Datye, K.H.: Effect of strut thickness, crimping and expansion diameters on radial strength, recoil and foreshortening of a coronary stent. Department of Mechanical and Materials Engineering, Florida International University. Miami. (Cited on pages 12, 13, 15, and 16.)

[23] Hibbeler, R.: *Mechanics of Materials. 2nd Edition*. Macmillan, 1994. (Cited on page 15.)

[24] Kastrati, A., Dirschinger, J. and Boekstegers, P.: Influence of stent design on 1-year outcome after coronary stent placement, a randomized comparison of five stent types in 1147 unselected patients. *Catheterization Cardiovascular Intervention*, vol. 50, pp. 290–297, 2000. (Cited on page 15.)

[25] Barth, K., Froelich, J. and Virmani, R.: Paired comparison of vascular wall reactions to palmaz stents, strecker tantalum stents, and wallstents in canine iliac and femoral arteries. *Circulation*, vol. 93, pp. 2161–2169, 1996. (Cited on page 16.)

[26] CRTonline: Fda approves edwards's sapien heart valve trial. 2008.
Available at: `http://www.crtonline.org/pr.aspx?PAGE_ID=4057` (Cited on page 19.)

[27] Iso 5840 international standard for cardiac valve prostheses. 2005. (Cited on pages 21 and 22.)

[28] Chikwe, J., Walther, A. and Pepper, J.: The surgical management of aortic valve disease. *British Journal of Cardiology*, vol. 6, pp. 453–461, 2003. (Cited on page 25.)

[29] Lifeciences, E.: Edwards sapien transcatheter heart valve.
Available at: `http://www.edwards.com/products/percutaneousvalves/sapienthv.htm` (Cited on pages 30 and 95.)

[30] *Marc 2007 r1 - Volume B: Element Library*, . (Cited on page 35.)

[31] Visser, G.: E-mail correspondecse with author, 1 november 2007. (Cited on page 37.)

[32] Xia, Z., Ju, F. and Sasaki, K.: A general finite element analysis method for balloon expandable stents based on repeated unit cell (ruc) model. *Finite Elements in Analysis and Design*, vol. 43, pp. 649–658, 2007. (Cited on page 38.)

[33] Stuparu, M.: Human heart valves, hyperelastic material modeling. Tech. Rep., University of Timisoara, 2002. (Cited on page 38.)

[34] Mark, A.: Applications of high pressure balloons in the medical device industry. Tech. Rep., Advanced Polymers Inc., 1999. (Cited on page 38.)

[35] J.E. Shigley, C.R.M. and Budynas, R.: *Mechanical Engineering Design: Seventh Edition*. McGraw-Hill Higher Education, 2003. (Cited on pages 51 and 56.)

[36] Marrey, Ramesh V, e.a.: Fatigue and life prediction for cobalt-chromium stents: A fracture mechanics analysis. *Biomaterials*, vol. 27, pp. 1988–2000, 2006. (Cited on pages 51 and 55.)

[37] Stainless, A.: Grades of stainless steel - grade 316. 2007.
Available at: `http://www.fanagalo.co.za/tech/tech_grade_316.htm` (Cited on page 55.)

[38] D. Aslanidis, G. Roebben, J.B. and van Moorleghem, W.: Electropolishing for medical devices: Relatively new... fascinatingly diverse. Tech. Rep., @medical technologies n.v. (AMT), 2001. (Cited on page 65.)

[39] Lehmann, M.: E-mail correspondence with author, 5 june 2008.: Stainless steel 316l stents - electropolishing procedure and electropolish composition. (Cited on page 65.)

[40] Dumoulin, C. and Cochelin, B.: Mechanical behaviour modelling of balloon-expandable stents. *Journal of Biomechanics*, vol. 33, pp. 1461–1470, 2000. (Cited on pages 74 and 94.)

[41] Johnson & johnson gateway.
Available at: `http://www.jnjgateway.com` (Cited on page 94.)

[42] David Chua, S., MacDonald, B. and Hashmi, M.: Finite-element simulation of stent expansion. *Journal of Materials Processing Technology*, vol. 120, pp. 335–340, 2002. (Cited on page 94.)

[43] Migliavacca, F.e.a.: Mechanical behavior of coronary stents investigated through the finite element method. *Journal of Biomechanics*, vol. 35, pp. 803–811, 2002. (Cited on page 94.)

Appendices

Appendix A

Stent Design Concepts

A.1 Stent Concept: Design 1

The concept for Design 1 was based on the Palmaz-Schatz [40; 41; 42; 43] coronay stent from Johnson & Johnson Medical Devices. This design consists of a tube with simple square slots which appear like diamond shaped cells after expansion. Figure A.1 and Figure A.3 respectively shows the undeformed initial geometry and fully expanded configuration of the stent. Due to the cyclic radial symmetry of the stent, the initial expansion, crimping and rigid deployment process was simulated for only one seventh of the stent. The results of the simulation was then revolved to show the complete stent. From Figure A.3 it can be seen that the stent has 14 distal protrusion annexes. However the three leaflets of the valve assembly require three assembly joints, equi-spaced around the diameter of the stent. For this reason, an ideal stent for the assembly must have a number of distal protrusion annexes which is a multiple of three. The total equivalent plastic strain after the deployment process is in excess of 60% (see Figure A.3) and the strain-limit of Stainless Steel 316L is 43%. Figure A.2 shows the crimped state of the stent. From the figure, it can be seen that the stent experiences severe non-uniform deformation during the crimping process. Given the factors discussed in the previous paragraph, it is apparent that this stent design is not suitable for a

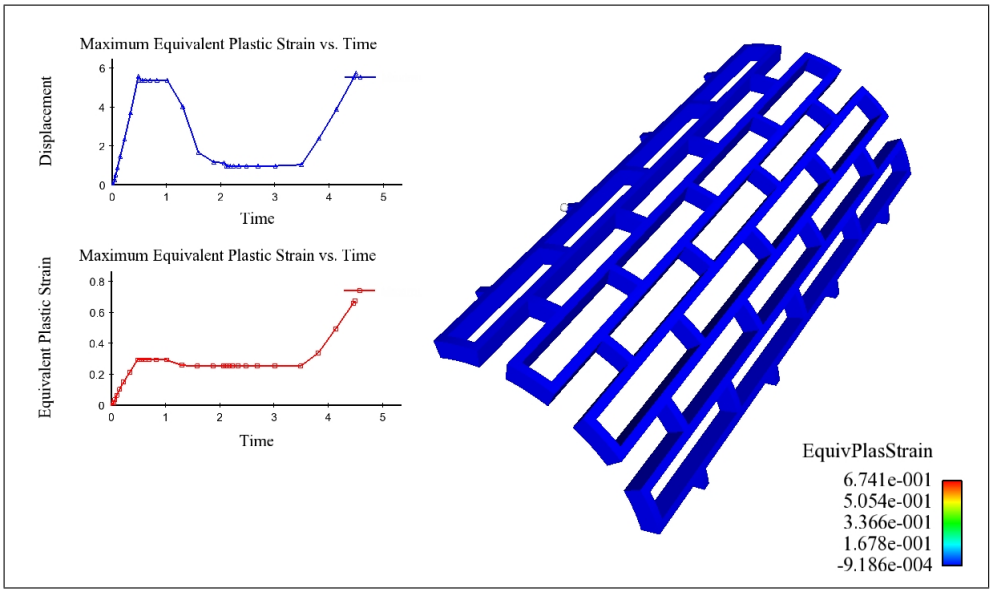

Figure A.1: Stent Design 1: Undeformed State

percutaneous aortic valve application, and the design was subsequently rejected as a feasible concept.

A.2 Stent Concept: Design 2

The concept for Design 2 was based on the stent used in the Edwards SAPIEN Transcatheter Heart Valve from Edwards Life Sciences [29]. This design consists of three support props, which serve as assembly joints for the three leaflets of the valve. The support props are connected with two sets of mirrored zig-zag shaped struts, which enable the crimping and expansion of the stent. Figure A.4 and Figure A.6 respectively shows the undeformed initial geometry and fully expanded configuration of the stent. Due to the cyclic radial symmetry of the stent, the initial expansion, crimping and rigid deployment process was simulated for only one third of the stent. The results of the simulation was then revolved to show the complete stent. It can be seen form Figure A.5, which indicates the crimped state of the stent, that the stent performs well under the crimping process. The design differs from the Edwards SAPIEN design

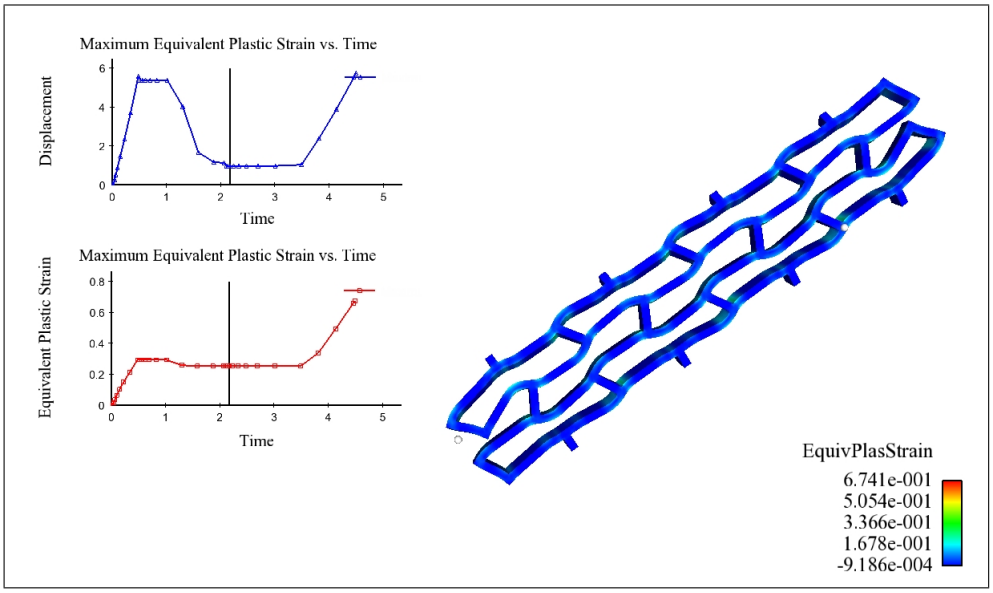

Figure A.2: Stent Design 1: Crimped State

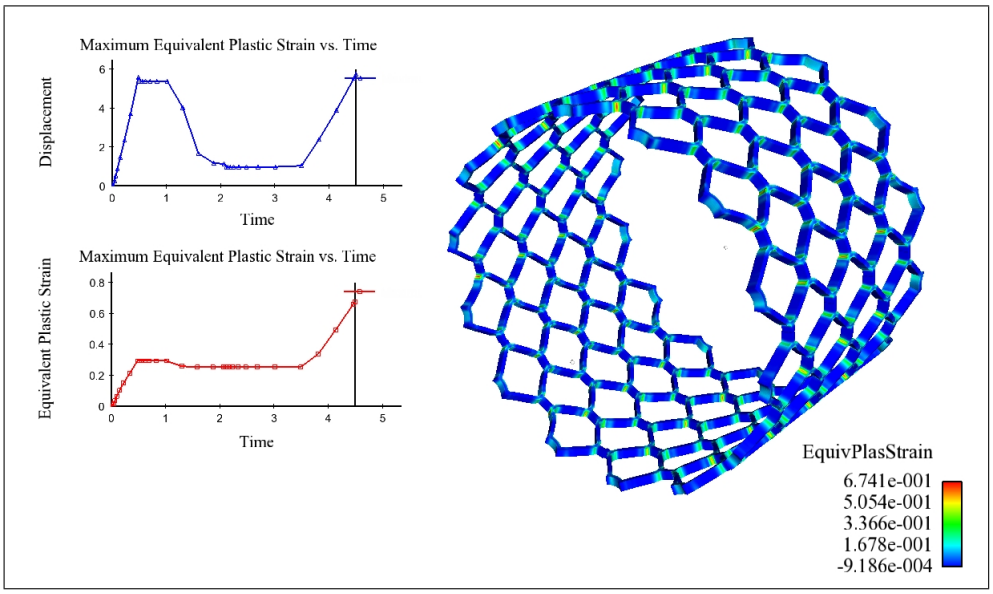

Figure A.3: Stent Design 1: Deployed State

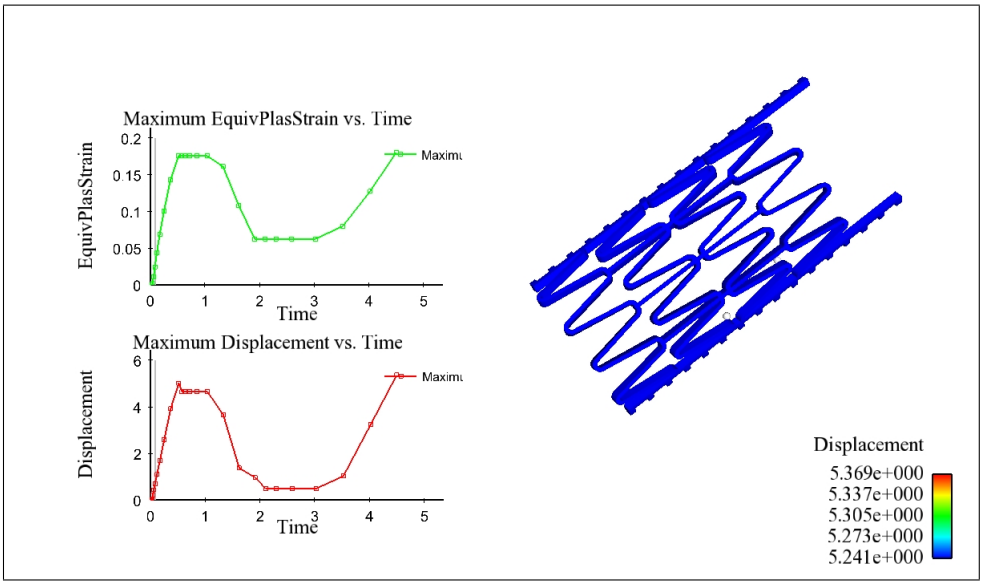

Figure A.4: Stent Design 2: Undeformed State

in that the support props extend well beyond the final row of stuts (See Figure A.4). This is to allow for a maximum stent length, while preventing coronary obstruction from the stent. Maximizing the stent length is advantageous as it allows for more room to seal the stent (which prevents regurgitation), given the minimum required stent length to assemble the valve leaflets. A simplified fatigue analysis was conducted of the predicted cyclic forces as experienced by the support props during the valve operation (Details of the fatigue analysis are given in section 5.8). Figure A.7 shows the maximum stress state of the fatigue analysis. The analysis indicated that the safety factor against fatigue was 1.15. Given that the required FSF was given as 1.5 (see section 3.1), this design did not conform to the engineering requirements and was subsequently rejected. None the less, the design served as the basis for further concept development.

A.3 Stent Concept: Design 3

The concept for Design 3 consists of a zig-zag strut pattern (along the stent circumference) which has been duplicated and translated along the

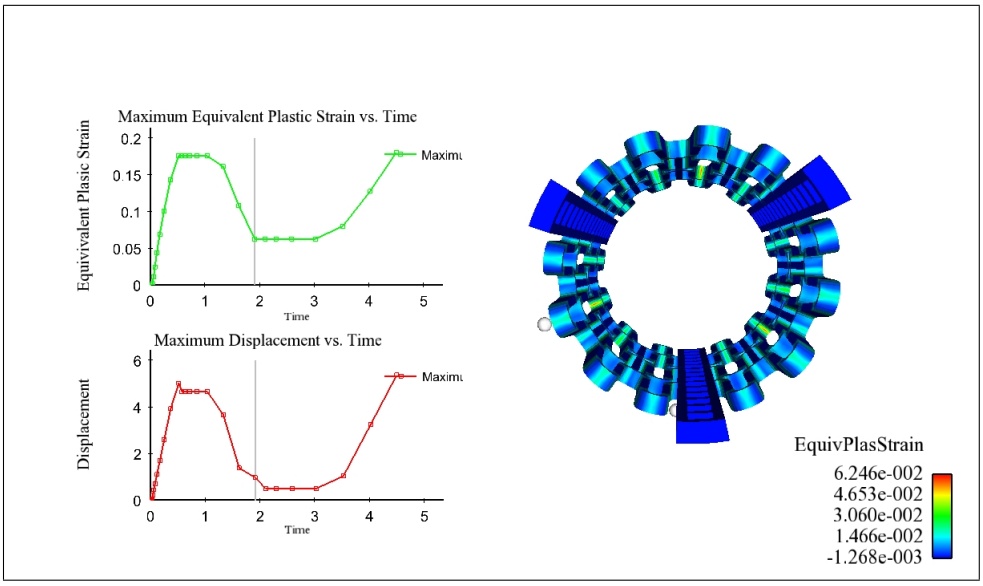

Figure A.5: Stent Design 2: Crimped State

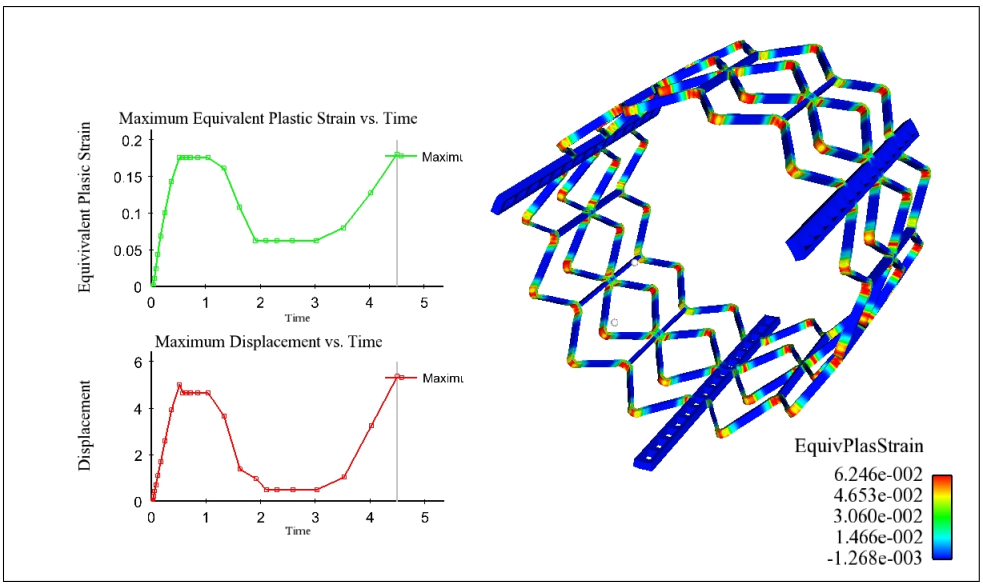

Figure A.6: Stent Design 2: Deployed State

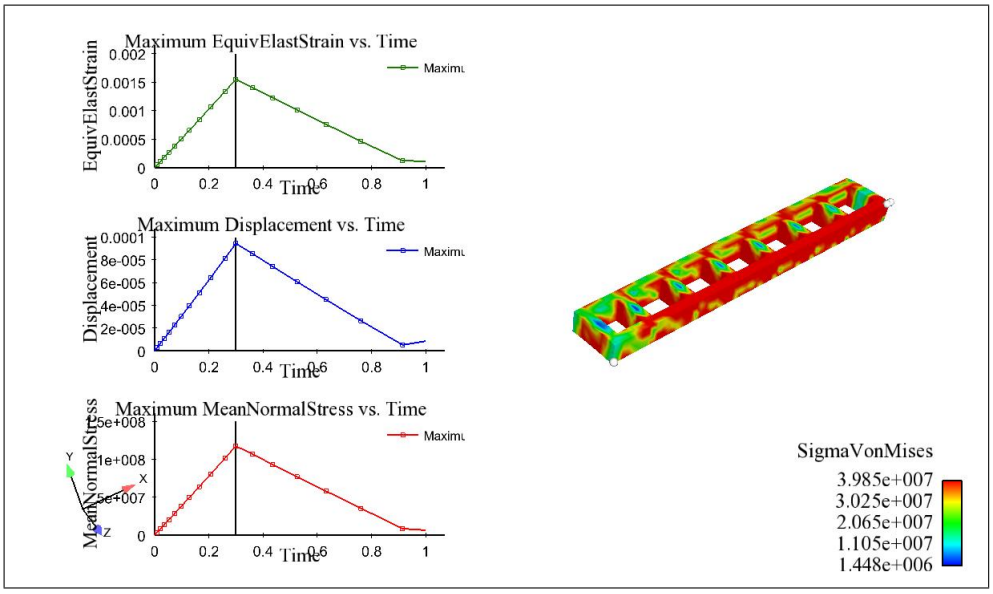

Figure A.7: Stent Design 2: Fatigue Analysis

axial direction. The zig-zag strut patterns are inter-connected with straight axial struts. The zig-zag strut pattern enables the crimping and expansion of the stent, while the straight struts provide the structural support for the stent. Figure A.8 and Figure A.10 respectively shows the undeformed initial geometry and fully expanded configuration of the stent. Due to the cyclic radial symmetry of the stent, the initial expansion, crimping and rigid deployment process was simulated for only one twelth of the stent. The results of the simulation was then revolved to show the complete stent. It can be seen form Figure A.9, which indicates the crimped state of the stent, that the stent performs well under the crimping process. The concept was more suitable for the *parabolic* leaflets as compared to the *straight* leaflets. However, the strut alignment at the deployed state was not ideal for a parabolic leaflet assembly. Given the stent-leaflet slight incompatibility, the stent concept was rejected.

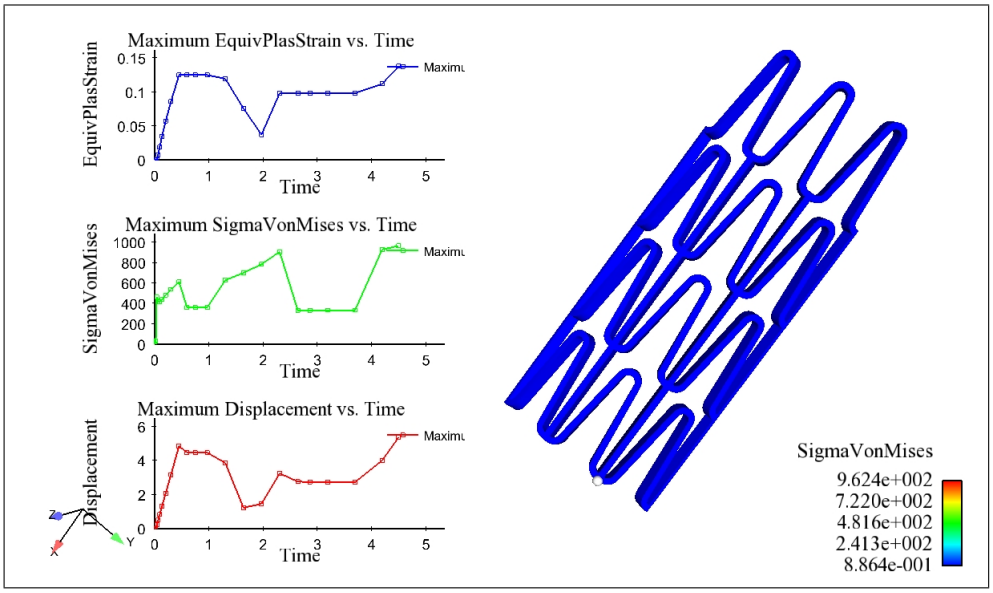

Figure A.8: Stent Design 3: Undeformed State

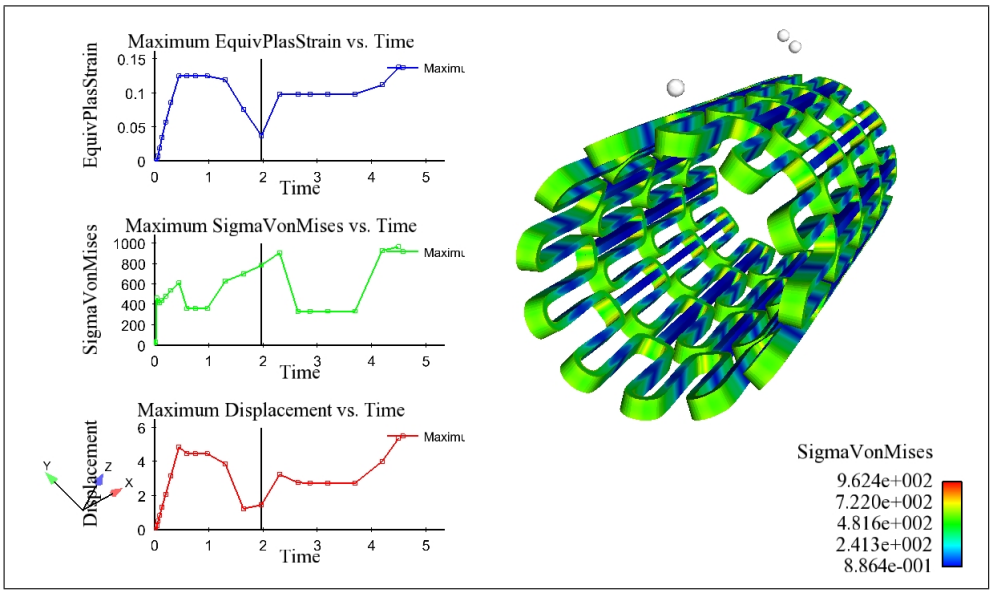

Figure A.9: Stent Design 3: Crimped State

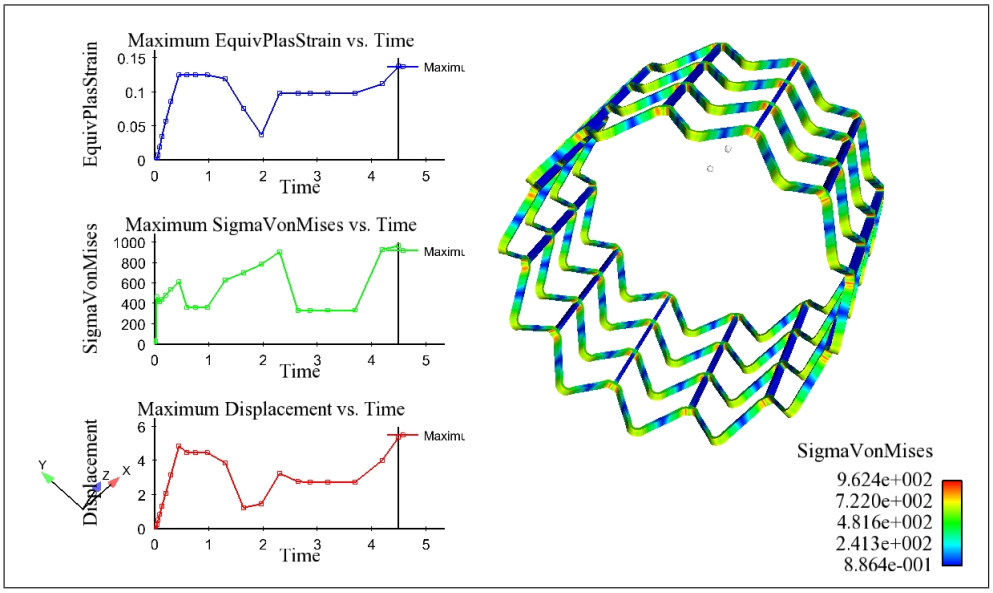

Figure A.10: Stent Design 3: Deployed State

Appendix B

FEM Boundary Conditions

B.1 Concept A

The red element faces in Figure B.1 indicate the planes of cyclic symmetry for Concept A. The nodes in the planes of cyclic symmetry were constrained to only allow for axial and radial translation in the symmetry planes. The orange marker indicates the node that was subjected to axial constraints to prevent the rigid body translation of the model.

B.2 Concept B

The red element faces in Figure B.2 indicate the planes of cyclic symmetry for Concept B. The nodes in the planes of cyclic symmetry were constrained to only allow for axial and radial translation in the symmetry planes. The orange marker indicates the node that was subjected to axial constraints to prevent the rigid body translation of the model.

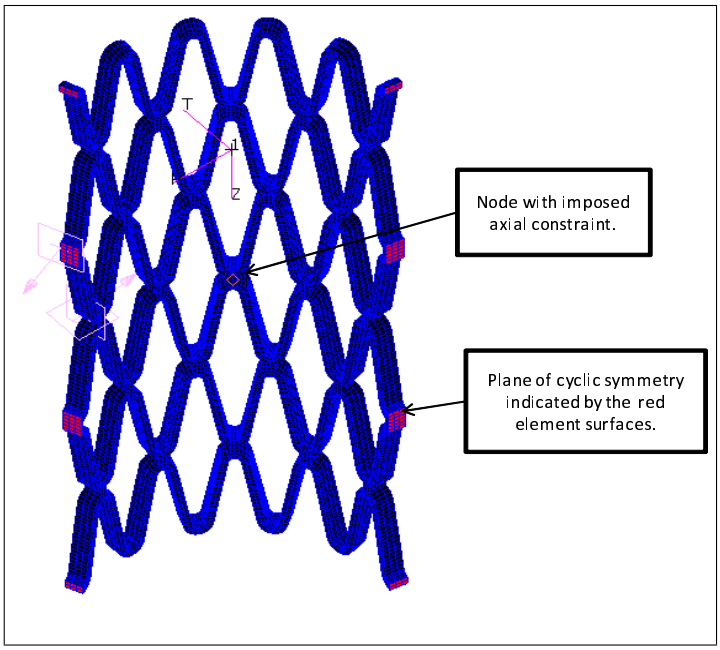

Figure B.1: Concept A: Displacement Constraints

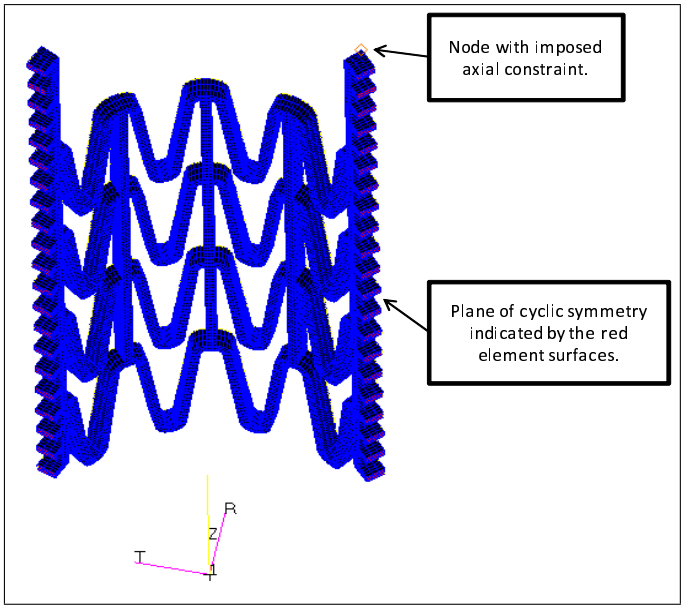

Figure B.2: Concept B: Displacement Constraints

Appendix C

Concept B - Load Steps

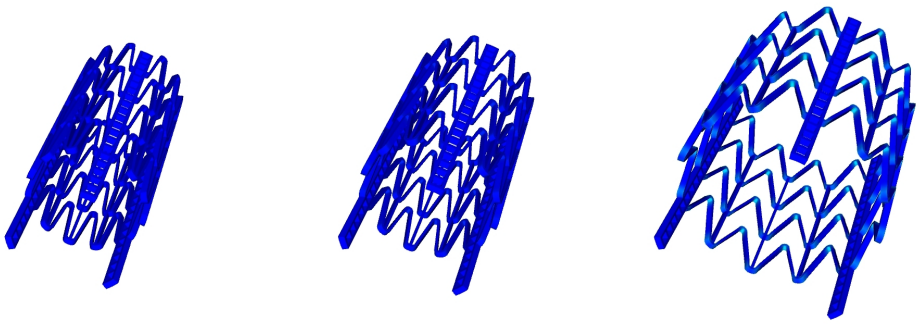

Figure C.1: Assembly Expansion Load Step

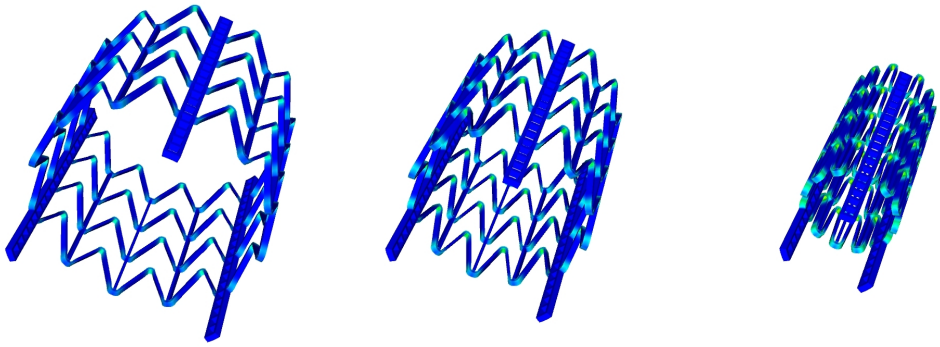

Figure C.2: Crimping Load Step

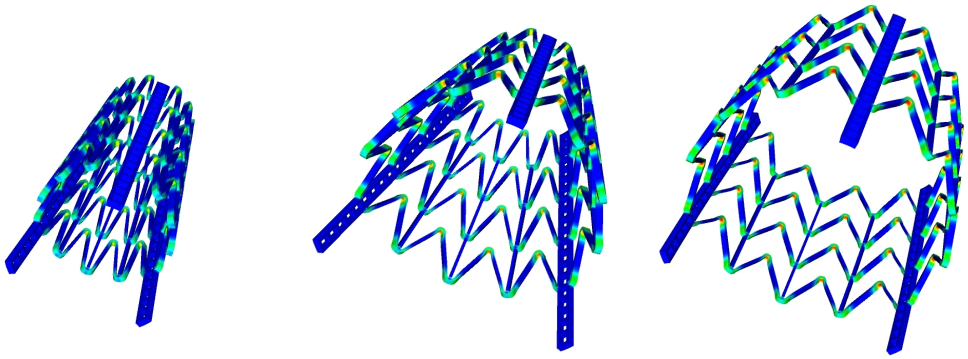

Figure C.3: Deployment Load Step

Appendix D

Electropolished Samples

Figure D.1 shows a magnified image of an untreated tubing sample. Figures D.2 to D.9 shows magnified images of tubing samples that were electropolished, each with different parameters. The parameters that were used for each sample is given in table D.1.

Figure D.1: Untreated Sample

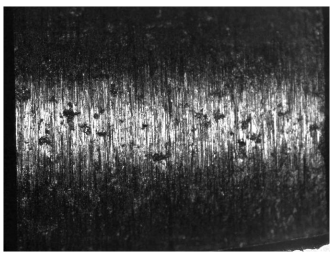

Figure D.2: Sample 1

Figure D.3: Sample 2

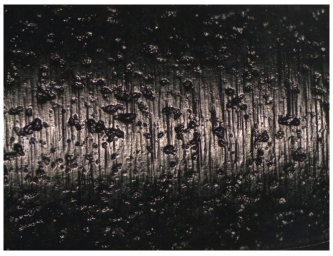

Figure D.4: Sample 3

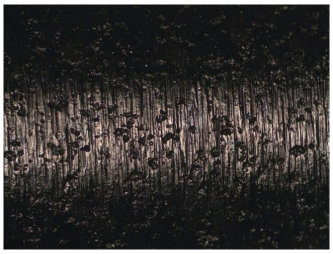

Figure D.5: Sample 4

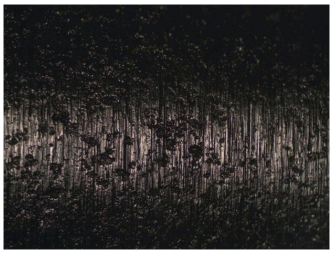

Figure D.6: Sample 5

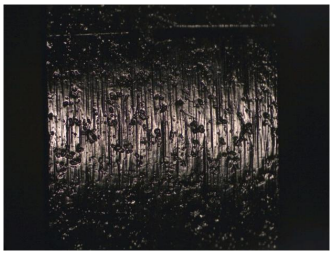

Figure D.7: Sample 6

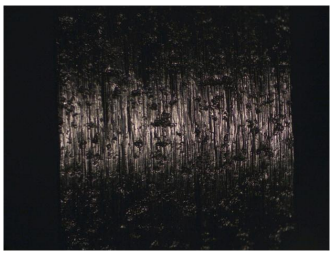

Figure D.8: Sample 7

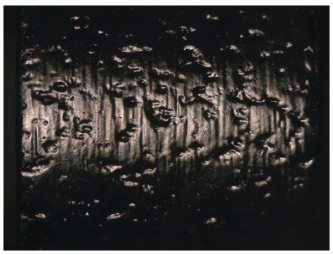

Figure D.9: Sample 8

Table D.1: Electropolished Sample Tubing: Parameters

	Voltage (V)	Agitation	Temperature (Degrees)	Processing Time (s)
Sample 1	16	3/6	72	90
Sample 2	16	3/6	70	120
Sample 3	16	3/6	70	135
Sample 4	16	3/6	80	75
Sample 5	16	3/6	72	150
Sample 6	16	3/6	73	120
Sample 7	16	3/6	72	105
Sample 8	16	3/6	88	135

Appendix E

Fatigue Analysis: MATLAB Code

```
clear all
close all

%Load MSC.Marc Report File
load CoreValve_fatigue_020.rpt;

%Write File to Variable
data = CoreValve_fatigue_020(:,3);

%Declare Variables

    %Number of Timesteps
Timesteps = 19;

    %Number of Elements
Elements = length(data)/19;

    %Fatigue Limit
sigma_e = 260;

    %True Ultimate Tensile Strength
```

```
sigma_ut = 965;

%Organise Data into Columns
for ii = 0:Elements - 1
for jj = 1:Timesteps
data1(jj,ii+1) = data(ii*9+jj);
end
end

%Get max and min principle stresses for each element
for ii = 1:Elements
max_prin_stress(ii) = max(data1(:,ii));
min_prin_stress(ii) = min(data1(:,ii));
end

%Calculate mean stress ans stress ampliture for each element
for ii = 1:Elements
stress_mean(ii) = (max_prin_stress(ii)+min_prin_stress(ii))/2;
stress_amp(ii) = abs((max_prin_stress(ii)-min_prin_stress(ii))/2);
end

%Ignore Elements in Compression
jj = 1;
for ii = 1:Elements
if stress_mean(ii) >= 0
stress_mean1(jj) = stress_mean(ii);
stress_amp1(jj) = stress_amp(ii);
jj = jj + 1;
end
end

%Calculate Modified Goodman line
m = -sigma_e/sigma_ut;
```

```
x = 0:sigma_ut;
y = m*x + sigma_e;

%Calculate Data Point Nearest to Goodman Line
for ii = 1:length(stress_mean1)
c = stress_amp1(ii) - (-m)*stress_mean1(ii);
x1 = (c-260)/(2*m);
y1 = -m*x1+c;
dist(ii) = sqrt(((stress_amp1(ii)-y1)^2+(stress_mean1(ii)-x1)^2));
end

    %Calculate min distance
min_dist = min(dist);

    %Position of worst case data point
position = find(dist == min_dist);
    %Worst Case Mean Stress
wc_stress_mean = stress_mean1(position)

    %Worst Case Stress Amplitude
wc_stress_amp = stress_amp1(position)

%Get Worst Case Element Number
wc_Element = find(stress_mean == wc_stress_mean)

%Calculate Safety Factor Against Fatigue
SF = 1/((wc_stress_amp)/(260)+(wc_stress_mean)/(965))

%Plot Data and Write Figure to 'eps' file
plot(stress_mean1,stress_amp1,'.','markersize',4); %Plot Data
hold on
plot(x,y,'r','linewidth',2);
grid on
```

```
xlabel('Predicted Mean Stress (MPa)');
ylabel('Predicted Stress Amplitude (MPa)');
legend('FEM Data','Modified Goodman Line');
plot(wc_stress_mean,wc_stress_amp,'x','markersize',6);
print('-depsc','-r600','CoreValve020.eps')
```

Appendix F

Fatigue Analysis: Results

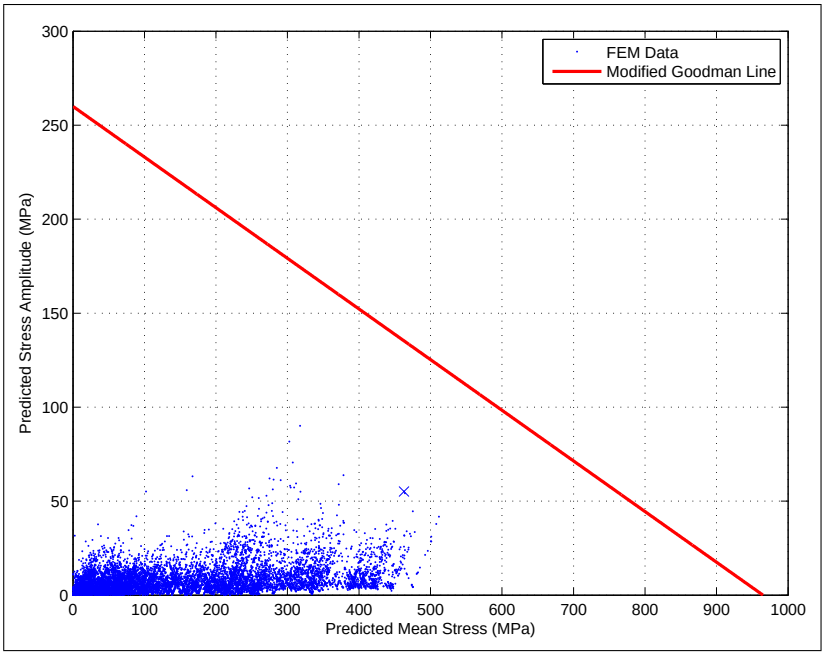

Figure F.1: Concept A: Fatigue Diagram - Strut Width 0.20 mm

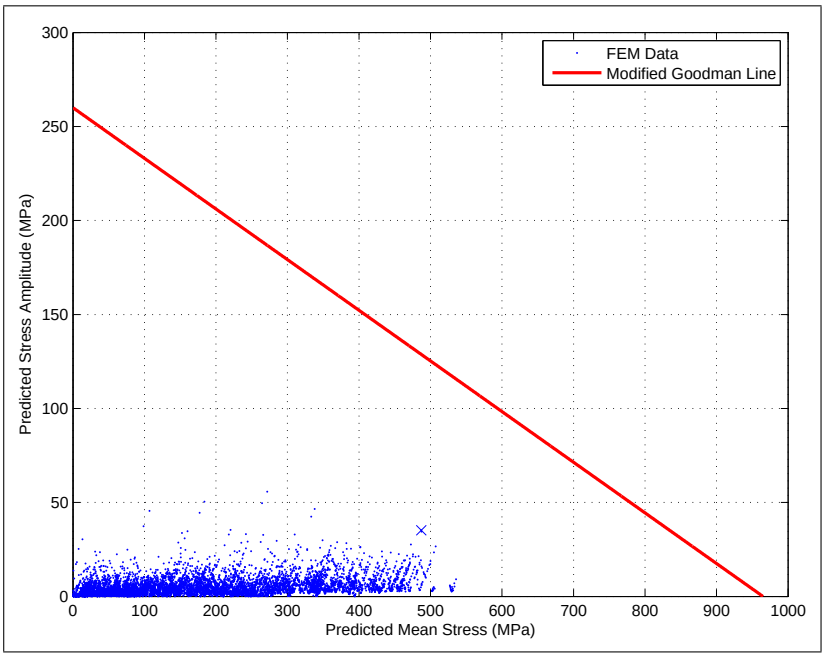

Figure F.2: Concept A: Fatigue Diagram - Strut Width 0.25 mm

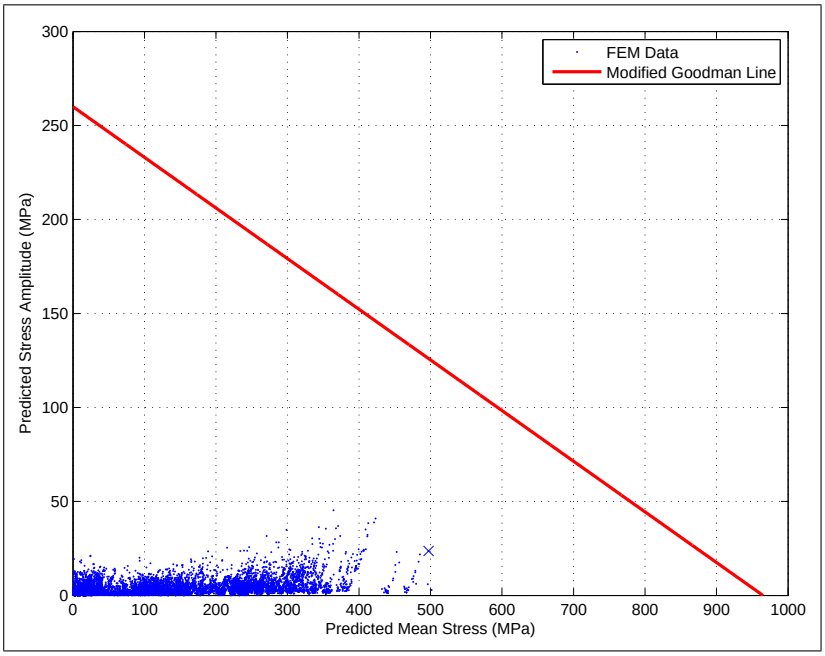

Figure F.3: Concept A: Fatigue Diagram - Strut Width 0.27 mm

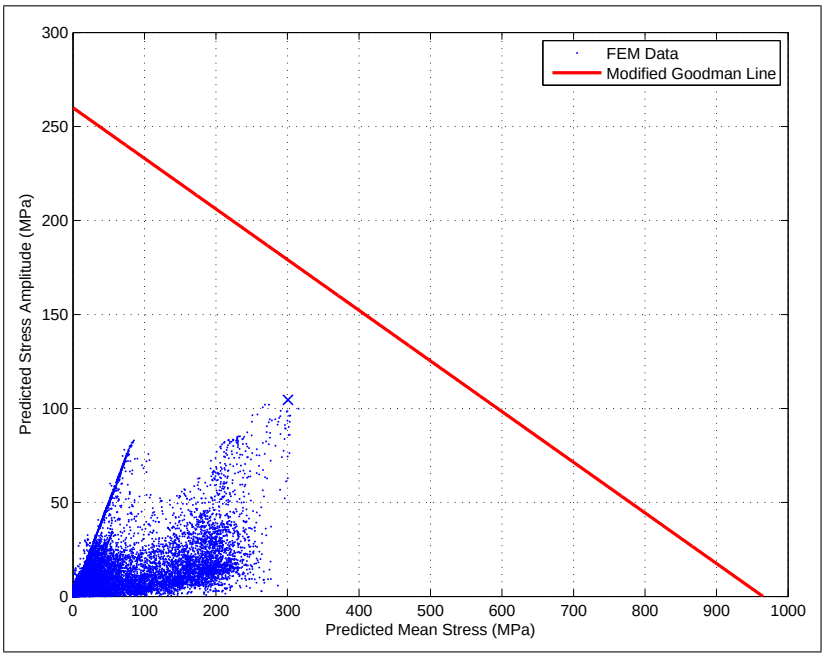

Figure F.4: Concept B: Fatigue Diagram - Strut Width 0.20 mm

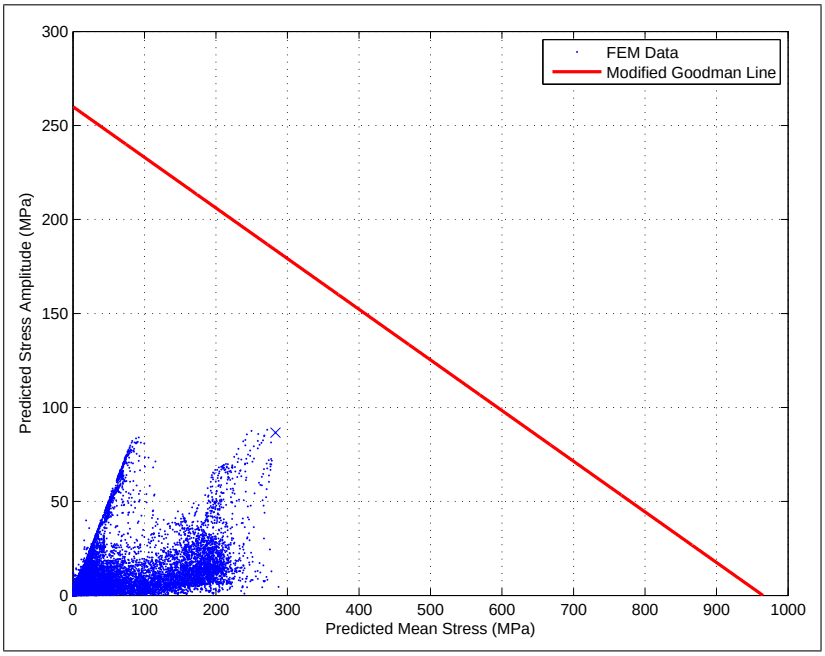

Figure F.5: Concept B: Fatigue Diagram - Strut Width 0.22 mm

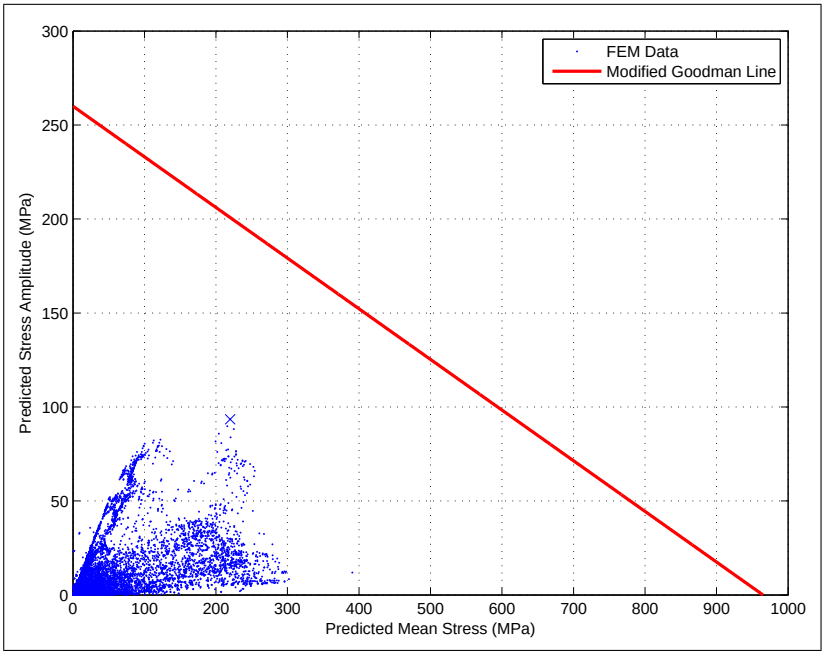

Figure F.6: Concept B: Fatigue Diagram - Strut Width 0.27 mm

Appendix G

Concept A: Second Iteration

Figure G.1 shows the suggested dimensions for the second iteration of Concept A.

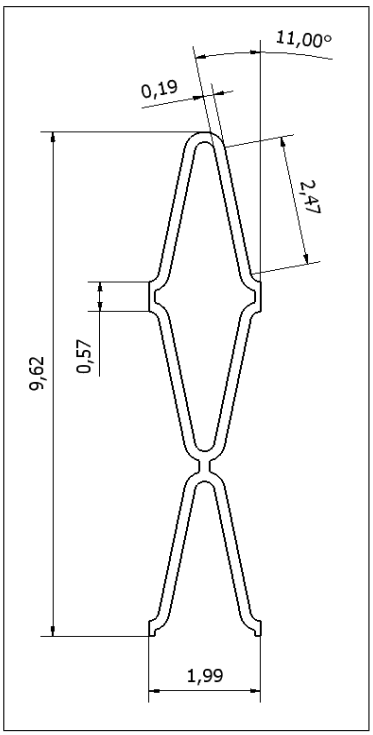

Figure G.1: Concept A: Second Iteration